PHYSICAL REVIEW D **96,** 014506 (2017)

Improved lattice computation of proton decay matrix elements

Yasumichi Aoki,[1,2] Taku Izubuchi,[2,3] Eigo Shintani,[4] and Amarjit Soni[3]

[1]*High Energy Accelerator Research Organization (KEK), Tsukuba 305-0801, Japan*
[2]*RIKEN-BNL Research Center, Brookhaven National Laboratory, Upton, New York 11973, USA*
[3]*High Energy Theory Group, Brookhaven National Laboratory, Upton, New York 11973, USA*
[4]*RIKEN Advanced Institute for Computational Science, Kobe, Hyogo 650-0047, Japan*

(Received 8 May 2017; published 14 July 2017)

We present an improved result for the lattice computation of the proton decay matrix elements in $N_f = 2+1$ QCD. In this study, by adopting the error reduction technique of all-mode-averaging, a significant improvement of the statistical accuracy is achieved for the relevant form factor of proton (and also neutron) decay on the gauge ensemble of $N_f = 2+1$ domain-wall fermions with $m_\pi = 0.34$–0.69 GeV on a 2.7 fm^3 lattice, as used in our previous work [1]. We improve the total accuracy of matrix elements to 10–15% from 30–40% for $p \to \pi e^+$ or from 20–40% for $p \to K\bar{\nu}$. The accuracy of the low-energy constants α and β in the leading-order baryon chiral perturbation theory (BChPT) of proton decay are also improved. The relevant form factors of $p \to \pi$ estimated through the "direct" lattice calculation from the three-point function appear to be 1.4 times smaller than those from the "indirect" method using BChPT with α and β. It turns out that the utilization of our result will provide a factor 2–3 larger proton partial lifetime than that obtained using BChPT. We also discuss the use of these parameters in a dark matter model.

DOI: 10.1103/PhysRevD.96.014506

I. INTRODUCTION

Although proton decay has yet to be observed experimentally, it is an important key observable in the search for new physics beyond the Standard Model (SM). The observed proton lifetime—i.e., $\tau_p > 8.2 \times 10^{33}$ years for $p \to \pi^0 e^+$ [2] (recently $\tau_p > 1.4 \times 10^{34}$ years was reported in Ref. [3]) or $\tau_p > 5.9 \times 10^{33}$ years for $p \to K^+\bar{\nu}$ [4]—imposes tight constraints on the parameter space of grand unified theories (GUTs) and supersymmetric GUTs (SUSY-GUTs). Currently, such an experimental bound might exclude minimal SU(5) GUTs, and SUSY-GUT models have been attractive as potential solutions of the hierarchy problem and the coupling unification of the SM at the GUT scale ($\sim 10^{16}$ GeV). SUSY-GUTs will favor the $p \to K^+\bar{\nu}$ decay channel within the detectable region of proton decay in future experiments (e.g., Hyper-Kamiokande [5]).

The main mode of proton decay through GUTs involves a proton decaying into a pseudoscalar meson and an antilepton. The operator product expansion (OPE) leads to the decay amplitude of such processes written in terms of the Wilson coefficients which contain all the details of the high-energy part of a GUT, and the low-energy QCD matrix elements of the proton and pseudoscalar states with three-quark operators. Each QCD matrix element is further decomposed into two form factors, called the relevant and irrelevant form factors. Denoting the relevant form factor as W_0, the partial decay width reads

$$\Gamma(N \to P + \bar{l}) = \frac{m_N}{32\pi}\left[1 - \left(\frac{m_P}{m_N}\right)^2\right]^2 \left|\sum_I C^I W_0^I(N \to P)\right|^2 + O(m_l/m_N), \quad (1)$$

with m_N, m_P, and m_l being the mass of the nucleon, pseudoscalar meson, and antilepton, and C^I being the Wilson coefficient of the operator of type I (distinguishing flavor and chiral structure), which also enters in W_0^I. Parameters in a given GUT model are encoded in the Wilson coefficients C^I. The knowledge of the left-hand side (experiment) and that of W_0 reported in this work will be transcribed into the knowledge of the GUT parameters, namely, the proton lifetime bound restricts the GUT parameters [6–24].

The relevant form factors are evaluated in the $\overline{\text{MS}}$ scheme in the naive dimensional regularization at a typical hadronic scale $\mu = 2$ GeV. The matching Wilson coefficients need to be calculated in the same way.[1]

The lattice computation of the proton decay matrix elements has a rather long history. It started with the calculation of the low-energy constants (LECs) α and β in the quenched approximation $N_f = 0$, where one needs to use a baryon chiral perturbation theory [25] to obtain W_0. The uncertainties of these initial computations [26–28] were successively reduced with systematic improvements by employing the direct method [1,29,30], the continuum limit of LECs with $N_f = 0$ [31], nonperturbative renormalization with the chirally invariant lattice formulation [1,30,32], LECs computed with $N_f = 2+1$ [32], and finally the computation of W_0 with $N_f = 2+1$ (see Table VI).

[1]In this study we estimate to one higher order in m_l/m_N for the antimuon final states. Simply replacing W_0 with W_μ, which is described later, will provide the partial decay width which is good to $O(m_\mu/m_N)$.

In our previous report [1], W_0 was calculated using the direct method with a proper dynamical fermion computation using the $N_f = 2 + 1$ domain-wall fermion formulation. There, the result for W_0 was reported with all of the relevant systematic uncertainties removed or properly estimated. However, the precision was not satisfactory because W_0 for the pion and kaon final-state matrix elements had 20–40% errors. Noticing that the fractional error gets doubled in the partial decay width as it enters quadratically in Eq. (1), it is necessary to have more precise results for W_0 in order to make them more useful.

A recent development of the algorithm to speed up the measurement of the matrix element in lattice QCD—called all-mode-averaging (AMA) [33–35]—enables us to further improve the statistical precision of the proton decay matrix element for the pion and kaon final states. This paper shows the update of the lattice calculation of the proton decay matrix element, in both "direct" and "indirect" measurements, for all decay modes on the same gauge ensembles as those used in Ref. [1]. As a consequence of increasing statistical accuracy, a more reliable estimate of the systematic error can be realized.

In addition, we previously did not take into account the muon mass effect for the case of a muon final state because the effect is subdominant compared to other uncertainties. However, with increased statistical accuracy, the effect of a nonzero muon mass (106 MeV) is visible. We provide the form factors for the muon final state separately from those with positron or neutrino final states.

Here we also attempt to use our lattice computation as an input for the proton decay matrix element for a model of dark matter [36–38]. Although the kinematics of our lattice setup is not so optimal, we can provide useful information for such a dark matter model as by-products.

This paper is organized as follows. After presenting the notation (Sec. II) and simulation parameters (Sec. III), we show the updated result of the lattice evaluation of the low-energy constants α and β in baryon chiral perturbation theory (BChPT) for the indirect method in Sec. IV, and the relevant form factor W_0 of proton decay in Sec. V. In Sec. V we also make an assessment of the unestimated systematic error in the indirect method and focus on their use in the estimate of the proton lifetime. A description of how our results can be used in a dark matter model [36–38] is given in Sec. VI. A test of the soft-pion theorem of our lattice results is shown in Appendix B. Throughout the paper dimensionful quantities are expressed in lattice units and the lattice spacing "a" is suppressed in equations.

II. PROTON DECAY MATRIX ELEMENT

The lattice calculation is concentrated on the QCD matrix element of the $N \to P$ transition, in which N denotes the nucleon (proton or neutron) and P is one of the pseudoscalars from the π^0, $\pi^\pm$, K^0, K^+ or η meson. At the hadronic energy scale, only the lowest-dimensional operators with baryon number violation are relevant. They are the dimension-six four-fermi (three quarks and one lepton) operators [39–41]. Since the on-shell lepton can be omitted from the QCD matrix element, the transition form factor from a nucleon $N(k)$ state (source field) to a meson $P(p)$ state (sink field) with a momentum transfer $q = k - p$ is represented as

$$\langle P(p)|\mathcal{O}^{\Gamma\Gamma'}(q)|N(k,s)\rangle = P_{\Gamma'}\left[W_0^{\Gamma\Gamma'}(q^2) - \frac{i\not{q}}{m_N}W_1^{\Gamma\Gamma'}(q^2)\right]u_N(k,s). \quad (2)$$

For the physical kinematics $-q^2 = m_l^2$, the contribution of the W_1 term is relatively small compared to the W_0 term, due to the suppression prefactor m_l/m_N. In $m_l = e^+$ or $\bar{\nu}$, W_0 is only relevant to the proton decay matrix element since the second term is $m_e/m_N \sim \mathcal{O}(10^{-3})$, while in the $m_l = m_\mu$ case, because $m_\mu/m_N \sim \mathcal{O}(10^{-1})$, the contribution of the W_1 term to the matrix element is not negligible for our target precision (below 10% precision). Namely, we define

$$W_\mu \equiv W_0(-m_\mu^2) + \frac{m_\mu}{m_N}W_1(-m_\mu^2). \quad (3)$$

We estimate W_0 and W_1 and provide $W_0(q^2 = 0)$ for the positron and neutrino final states and W_μ for the antimuon final states. The baryon-number-violating three-quark operator $O^{\Gamma\Gamma'}$ reads

$$O^{\Gamma\Gamma'} = U_{\Gamma\Gamma'}\varepsilon^{ijk}(q^{iT}CP_\Gamma q^j)P_{\Gamma'}q^k, \quad (4)$$

with the chiral projection $P_\Gamma = (1 \pm \gamma_5)/2$, where "+" is for $\Gamma = R$ and "−"is for $\Gamma = L$. q^i is the quark flavor (up, down, or strange) with color index i. $U_{\Gamma\Gamma'}$ denotes the renormalization factor which was already computed using the nonperturbative method [32].[2] Using the symmetry of parity transformation between different chirality combinations ($RL \Leftrightarrow LR$ or $LL \Leftrightarrow RR$) [30] enables us to reduce four chirality combinations to two combinations: $\Gamma\Gamma' = LL$ and RL. Applying the exchange symmetry of u and d, we have the equivalence of matrix elements between the proton and neutron,

$$\langle\pi^0|(ud)_\Gamma u_{\Gamma'}|p\rangle = \langle\pi^0|(du)_\Gamma d_{\Gamma'}|n\rangle, \quad (5)$$

[2]Recently, we found an error in our one-loop perturbative formula which is used for matching between the $\overline{\text{MS}}$ scheme with the naive dimensional regularization and the RI-SMOM renormalization scheme [Eq. (C.8) in Ref. [30] and Eq. (46) in Ref. [32]]. (We thank Michael Buchoff and Michael Wagman for pointing out that mistake.) After correcting this error, the impact of all matrix element calculations is increased by about 6–7% for α, β, and W_0 [30,32,42]. In this paper we use the corrected value as presented in Eq. (18).

TABLE I. Lattice ensemble set and parameters. m refers to the domain-wall fermion mass for the degenerate light quarks (u and d). N_g is the number of approximations using both light and strange quark propagators. $N_{\rm eig}$ denotes the number of low modes used in the light-quark propagator, and "res" is value of the squared norm of the residual vector for the sloppy solver in AMA. Values of hadron masses are measured with an extended quark source and sink with gauge-invariant Gaussian smearing.

a^{-1} GeV	m	m_π (GeV)	m_K (GeV)	m_N (GeV)	$N_{\rm eig}$	N_g	Res	$N_{\rm conf}$
1.7848(6)	0.005	0.340(1)	0.594(2)	1.179(5)	300	32	0.003	91
	0.01	0.427(1)	0.626(1)	1.269(5)	300	32	0.003	55
	0.02	0.574(1)	0.688(1)	1.452(4)	200	32	0.003	39
	0.03	0.694(1)	0.744(2)	1.598(5)	200	32	0.003	44

$$\langle\pi^+|(ud)_\Gamma d_{\Gamma'}|p\rangle = -\langle\pi^-|(du)_\Gamma u_{\Gamma'}|n\rangle, \tag{6}$$

$$\langle K^0|(us)_\Gamma u_{\Gamma'}|p\rangle = -\langle K^+|(ds)_\Gamma d_{\Gamma'}|n\rangle, \tag{7}$$

$$\langle K^+|(us)_\Gamma d_{\Gamma'}|p\rangle = -\langle K^0|(ds)_\Gamma u_{\Gamma'}|n\rangle, \tag{8}$$

$$\langle K^+|(ud)_\Gamma s_{\Gamma'}|p\rangle = -\langle K^0|(du)_\Gamma s_{\Gamma'}|n\rangle, \tag{9}$$

$$\langle K^+|(ds)_\Gamma u_{\Gamma'}|p\rangle = -\langle K^0|(us)_\Gamma d_{\Gamma'}|n\rangle, \tag{10}$$

$$\langle\eta|(ud)_\Gamma u_{\Gamma'}|p\rangle = -\langle\eta|(du)_\Gamma d_{\Gamma'}|n\rangle, \tag{11}$$

and furthermore, for the $p \to \pi$ channel, there is a relation in the SU(2) isospin limit, which is good for our target precision,

$$\langle\pi^+|(ud)_\Gamma d_{\Gamma'}|p\rangle = \sqrt{2}\langle\pi^0|(ud)_\Gamma u_{\Gamma'}|p\rangle. \tag{12}$$

Therefore, the total number of matrix element is 12. In this paper we show the 12 principal matrix elements of $\langle P|\mathcal{O}^{\Gamma L}|p\rangle$, for $\Gamma = R$ and L in lattice QCD.

Our target matrix element can be extracted from the computation of the ratio of the three-point and two-point functions. We use the same combination used in Eq. (21) of Ref. [42],

$$R_3^{\Gamma L}(t,t_1,t_0;\vec{p};P) = \frac{\mathrm{tr}[PC_{\mathcal{O}^{\Gamma L}}(t_1,t,t_0;\vec{p})]}{C_P(t_1,t;\vec{p})\mathrm{tr}[P_4 C_N(t,t_0)]}\sqrt{Z_P Z_N}, \tag{13}$$

where the nucleon two-point function $C_N(t,t_0)$ does not have momentum, and the pseudoscalar two-point function $C_P(t,t_0;p)$ has spatial momentum $\vec{p}$. Here we also use the two projection matrices $P = P_4 \equiv (1+\gamma_4)/2$ and $iP_4\gamma_j$. The three-point function $C_{\mathcal{O}^{\Gamma L}}(t_1,t,t_0;p)$ depends on $t-t_0$ (the time slice of the operator) and $t_s = t_1 - t_0$ (the source-sink separation), as well as the injected momentum $\vec{p}$ in the operator. The factors $\sqrt{Z_P}$ and $\sqrt{Z_N}$ are overlap factors of the pseudoscalar and nucleon states to their interpolating operators. Taking the trace of the two projection matrices P_4 and $iP_4\gamma_j$, the asymptotic form of this ratio can be expressed as a combination of W_0 and W_1,

$$\lim_{t_1-t,t-t_0\to\infty} R_3^{\Gamma L}(t,t_1,t_0;\vec{p},P_4) = W_0^{\Gamma L} + \frac{m_N - E_\pi}{m_N} W_1^{\Gamma L}, \tag{14}$$

$$\lim_{t_1-t,t-t_0\to\infty} R_3^{\Gamma L}(t,t_1,t_0;\vec{p},iP_4\gamma_j) = \frac{q_j}{m_N} W_1^{\Gamma L}, \tag{15}$$

and by solving the linear algebra we derive $W_0^{\Gamma L}$ and $W_1^{\Gamma L}$ simultaneously.

Calculating the three-point function $C_{\mathcal{O}^{\Gamma L}}(t_1,t,t_0;p)$ in Eq. (15) involves several steps. First, we compute the forward quark propagator with the nucleon source located at $t = t_0$ with a smeared source. Then, using the propagator at the meson sink position $t = t_1$, the sequential source computation is applied with an injection of momentum $\vec{p}$. Then, the obtained backward propagator is contracted at the operator position $t = t$ with two forward propagators from the nucleon source. This process needs $1 + N_p \times 2$ solver computations for each gauge configuration, with N_p being the number of different meson momenta. The factor of 1 is for a solver of the forward propagator, and the factor of 2 is for the solvers having the valence masses of the ud and s quarks. To achieve a good constraint on the fitting parameters, we need to have a good lever arm for m (different ensembles) and a variation of $\vec{p}$, which tends to lead to a large computational cost. The AMA technique [33–35,43] is useful for reducing the computational cost of the quark propagator. It enables us to carry out the high statistical measurement, even when using several momenta.

III. LATTICE SETUP

We use the same lattice gauge ensembles as in Refs. [42,44,45], which are generated with $N_f = 2+1$ domain-wall fermions (DWFs) and the Iwasaki gauge action at $\beta = 2.13$, corresponding to $a^{-1} = 1.7848(6)$ GeV [45] with a lattice size of $24^3 \times 64$ ($\simeq$2.65 fm^3). The four different quark masses $m = 0.005$, 0.01, 0.02, and 0.03

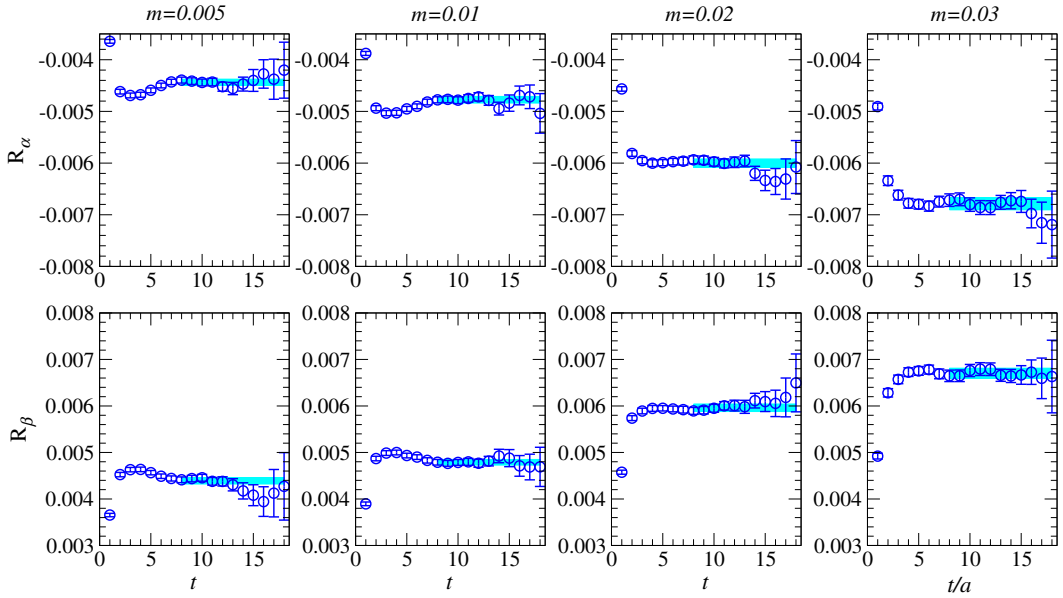

FIG. 1. $R_\alpha(t)$ (upper) and $R_\beta(t)$ (lower) as a function of lattice time slice. The cyan band denotes the line and statistical error of constant fitting within the fitting range.

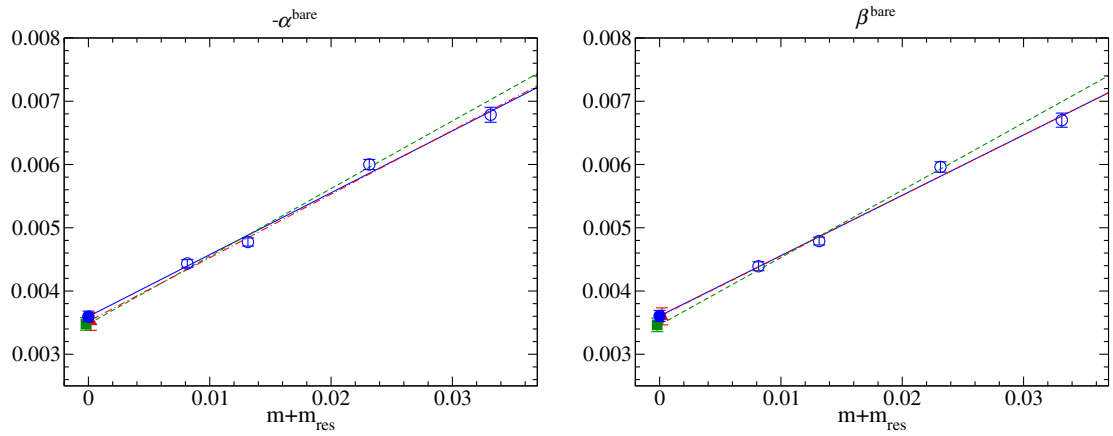

FIG. 2. Quark mass dependence of bare α and β. The straight lines are fits to the linear ansatz with three different fitting ranges: (i) containing all data [solid line (blue)], (ii) excluding the heaviest point [dashed-dotted line (red)], and (iii) excluding the lightest point [dashed line (green)] (see the text for details). Filled symbols represent the values in the chiral limit from the three fits.

are used at the unitary point, and the corresponding pion, kaon, and nucleon masses are given in Table I. In the measurement of the two-point function of the pseudoscalar meson and nucleon, we use the gauge-invariant Gaussian smeared source and sink function with the interpolation operator on APE-smeared link variable, whose parameter is the same as in Ref. [42]. For the "indirect" method, the two-point function including the baryon-number-violating operator [Eq. (4)] is computed using two nucleon source operators,

TABLE II. Error budget of α and β at $\mu = 2$ GeV. The "χ" column is the systematic uncertainty due to chiral extrapolation. The "a^2" column denotes the systematic uncertainty due to $\mathcal{O}(a^2)$. The "Δ_Z" and "Δ_a" columns are systematic uncertainties from the renormalization factor and lattice spacing.

LECs	Statistical error	Systematic error			
		χ	a^2	Δ_Z	Δ_a
$\alpha(\mathrm{GeV}^3) = -0.0144(15)$	0.0003	0.0005	0.0007	0.0012	0.0002
$\beta(\mathrm{GeV}^3) = 0.0144(15)$	0.0004	0.0005	0.0007	0.0012	0.0002

$$\mathcal{N}_5 = \varepsilon^{ijk}(u^{iT}C\gamma_5 d^j)u^k, \tag{16}$$

$$\mathcal{N}_{45} = \varepsilon^{ijk}(u^{iT}C\gamma_4\gamma_5 d^j)u^k, \tag{17}$$

which are then averaged. On the other hand, in the "direct" method for the two-point function in the ratio in Eq. (13), we use only $\mathcal{N}_5$ as the proton interpolation operator.

The renormalization factor needed to change the operators to those in the $\bar{\text{MS}}$ naive dimensional regularization (NDR) scheme at $\mu = 2$ GeV is calculated using the RI/MOM nonperturbative renormalization method combined with the RI/MOM $\to \bar{\text{MS}}$ matching factor calculated to next-to-leading order in perturbation theory. The renormalization factors of $\mathcal{O}^\Gamma$ with $\bar{\text{MS}}$ NDR at $\mu = 2$ GeV are given as

$$U^{RL} = 0.705(11)(56), \qquad U^{LL} = 0.706(11)(56), \tag{18}$$

where the first error is statistical and the second is systematic. The systematic error is dominated by the truncation error in perturbative matching, which is done to next-to-leading order. The estimate is from the size of $\alpha_s^2(\mu = 2\ \text{GeV})$ obtained from the renormalization-group-equation running starting from $\alpha_s(M_Z) = 0.1176(2)$ (see Ref. [30]).

In the computation of the three-point function, we use $t_s = 18$ ($\simeq$1.98 fm) for the source-sink separation, which is shorter than $t_s = 22$ ($\simeq$2.43 fm) used in Ref. [1]. Although using a short source-sink separation will suppress the statistical noise, we need to make sure the excited-state contamination is negligible. As the contamination would be more serious for smaller quark masses, we test such a contamination effect by comparing the ratio $R_3^{\Gamma L}$ for $t_s = 18$ and 22 at the lightest quark mass in Sec. IV.

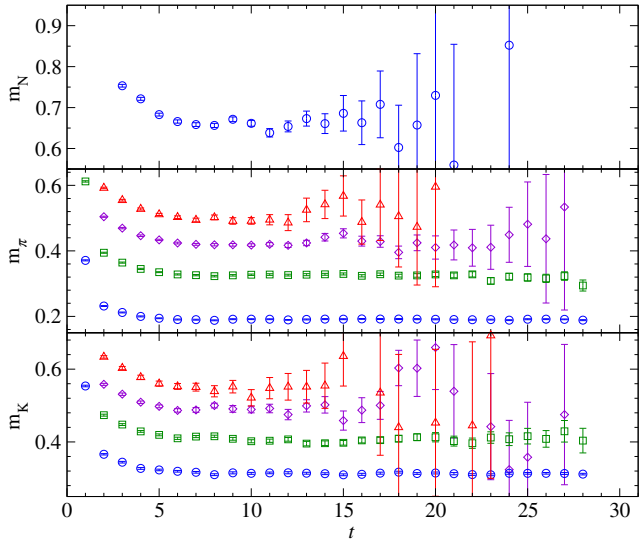

FIG. 3. Effective mass of the nucleon, pion, and kaon from the top to bottom panel. The different symbols denote data with different momentum values: zero (circle), $\vec{n}_p = (1,0,0)$ (square), $\vec{n}_p = (1,1,0)$ (diamond), and $\vec{n}_p = (1,1,1)$ (triangle). The quark mass is $m = 0.005$.

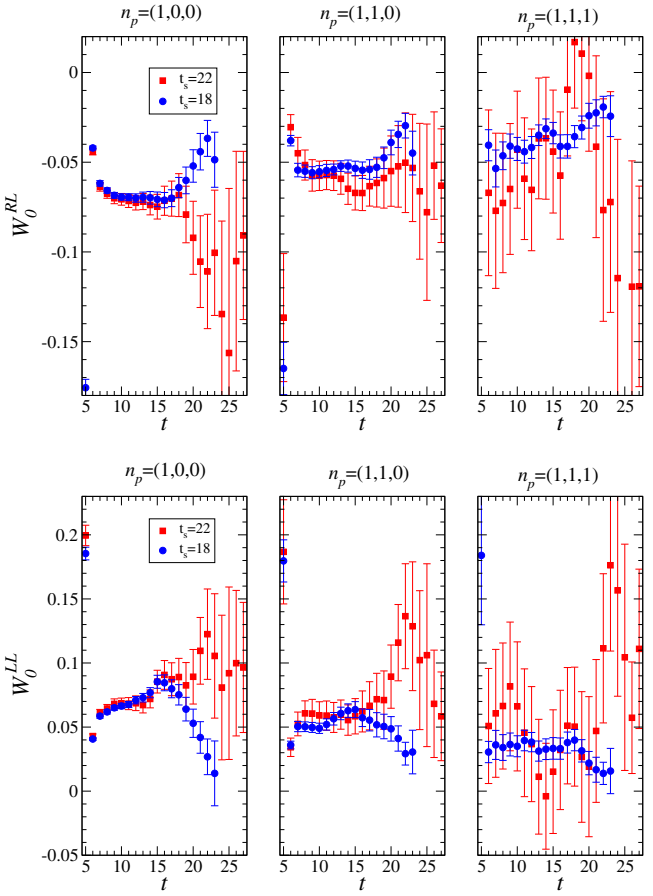

FIG. 4. Bare $W_0(t)$ for the $p \to \pi^0$ transition with $\Gamma = R$ (top) and $\Gamma = R$ (bottom) with $m = 0.005$. The different symbols represent results with $t_s = 22$ (red) and $t_s = 18$ (blue). The left, middle, and right panels are the results at the momenta $\vec{n}_p = (1,0,0)$, (1,1,0), and (1,1,1), respectively. The source nucleon ($t = 5$) and sink pion locations (27 or 23) have separations of 22 and 18, respectively.

We use three nonzero spatial momenta for the mesons, $\vec{p} = (1,0,0)$, (1,1,0), and (1,1,1), where the last one is a new addition from the previous study [1]. This will provide a good lever arm for the p^2 direction as well as a wide momentum range in the different kinematics (see Sec. VI).

The AMA technique is applied to the measurement of the three-point and two-point functions.[3] The low-mode deflation is used in solving the even-odd decomposed Dirac kernel with the conjugate gradient method. The corresponding low-mode is computed suing the Lanczos algorithm with Chebyshev polynomial acceleration, as

[3]For the two-point function $C_P(t_1, t; \vec{p})$ of the pion (or eta) in the denominator of Eq. (13), we have used a Kuramashi-wall source (as in Ref. [42]) for a heavier "light" quark mass, $m = 0.02$ and $m = 0.03$, since there is not much gain for cost reduction, and thus AMA was not applied in this case.

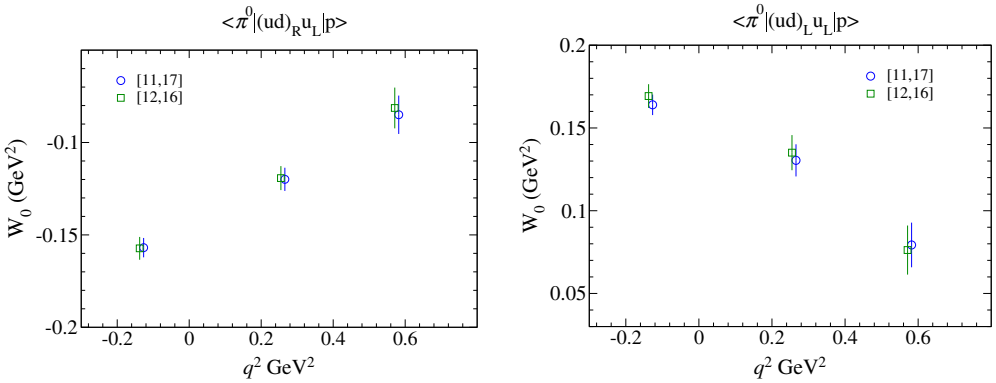

FIG. 5. Renormalized W_0 obtained from the plateau fit for data in Fig. 4 with three fitting ranges [13, 17], [11, 17], and [10, 18] with $m = 0.005$. The left panel is the result for $\Gamma = R$ and the right panel is the result for $\Gamma = L$ in the $p \to \pi$ channel.

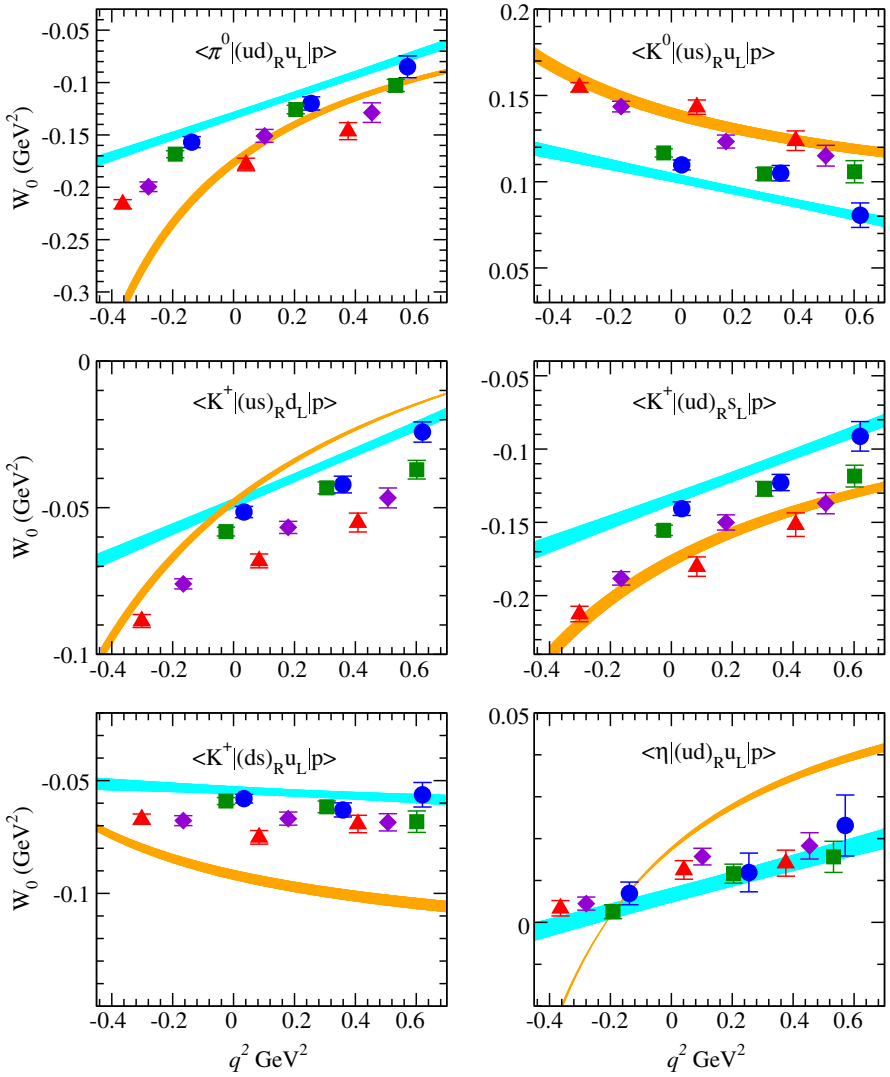

FIG. 6. Renormalized W_0 in the $\overline{\text{MS}}$ scheme with $\mu = 2$ GeV for $\Gamma = R$ in each channel. The different symbols are for $m = 0.005$ (circle), 0.01 (square), 0.02 (diamond), and 0.03 (triangle). We also show the chiral extrapolation line in the physical pseudoscalar mass as a cyan colored band. The orange colored band shows $W_0^{\alpha,\beta}$ including the central value and error of the LECs obtained in our calculation. These error bands only include the statistical error.

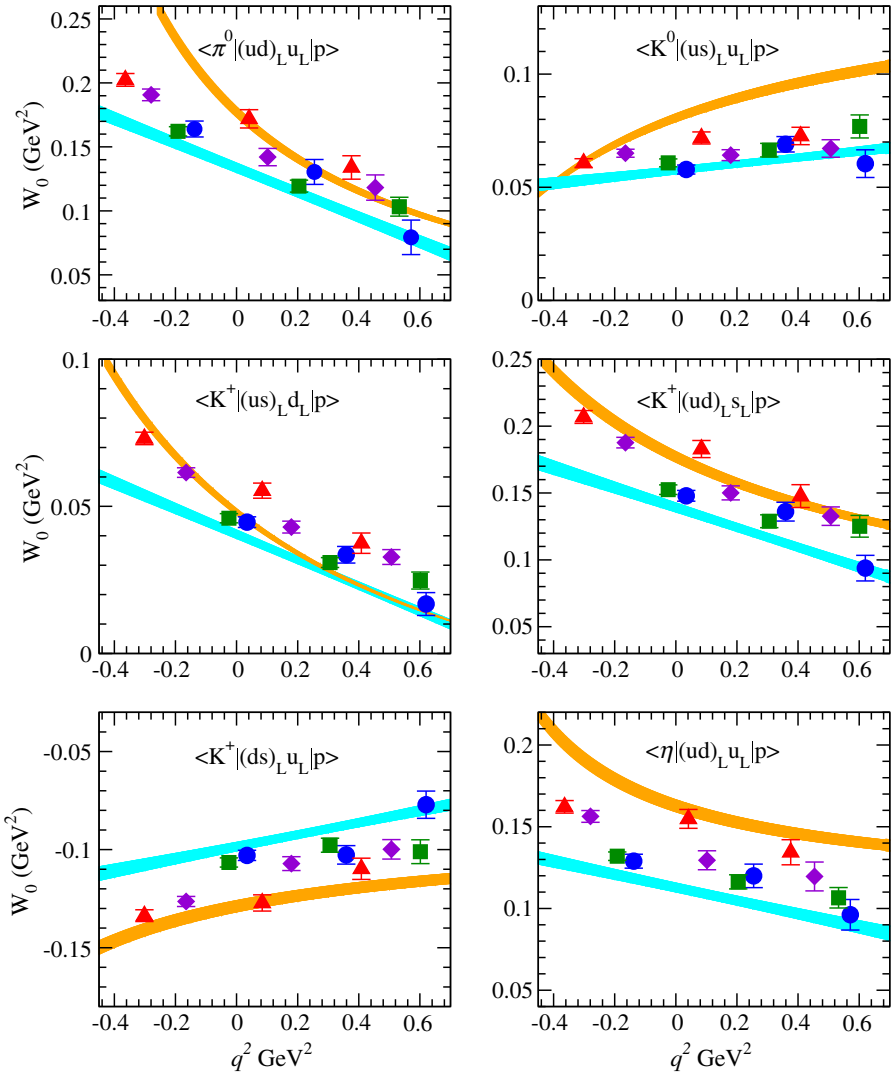

FIG. 7. Renormalized W_0 in the $\overline{\text{MS}}$ scheme with $\mu = 2$ GeV for $\Gamma = L$. Each symbol is the same as in Fig. 6.

performed in Ref. [35]. The number of low modes N_{eig} we computed for each quark mass are given in Table I. The approximation used in AMA is also constructed from the sloppy solver using a relaxed stopping condition (0.003 for the squared norm, which is compared to 10^{-8} for the "exact solve" done once every configuration). N_g shown in Table I is the number of such approximations we use in AMA. Note that in the strange quark mass we use a sloppy solver without deflation to avoid the additional computation of the low mode. Even without the low mode of the strange quark, AMA works rather well. Actually, we check that the correlation between the exact solution and the approximation is smaller than $1/N_g$.

IV. IMPROVED RESULT OF LOW-ENERGY CONSTANTS

First, we update the "indirect" measurement from the computation of LECs for the baryon-number-violating interaction in the chiral Lagrangian [25] following the method in Refs. [29–32,46]. In the "indirect" measurement, once corresponding LECs are obtained from lattice QCD (using BChPT together with the nucleon mass), couplings to the axial current (axial charge), the pion decay constant and its mass, and the proton decay amplitude can be evaluated. Each matrix element is proportional to the LECs depending on chirality: α (for RL) and β (for LL) [25,29]. These are defined through the nucleon-to-vacuum matrix elements. We write the quark flavor explicitly as

$$\langle 0|(ud)_R u_L|p\rangle = \alpha P_R u_p, \quad \langle 0|(ud)_L u_L|p\rangle = \beta P_L u_p, \quad (19)$$

with the proton spinor field u_p. The above matrix elements can be extracted from the ratio of the two-point function at large time-slice separation,

$$R_\alpha = \frac{C^R_{N\mathcal{O}}(t)}{C_N(t)} Z_N \xrightarrow{t\to\infty} \alpha, \quad R_\beta = \frac{C^L_{N\mathcal{O}}(t)}{C_N(t)} Z_N \xrightarrow{t\to\infty} \beta, \quad (20)$$

with the nucleon decay operator $\mathcal{O}$ and the nucleon interpolating operator having the same flavor content. The nucleon overlap factor Z_N is also calculated from the nucleon two-point function. From the practical point of view, this method is much cheaper than the "direct" method since α and β are obtained with a single computation of the quark propagator at each quark mass, whereas the direct method needs at least two additional propagators for each momentum value in the computation of the three-point function.

Figure 1 plots our results for $R_\alpha(t)$ and $R_\beta(t)$ obtained after averaging them with two different nucleon interpolating operators $\mathcal{N}_4$ and $\mathcal{N}_{45}$. Fitting to the plateau is done in the range $t \in [8, 18]$ for all cases, as shown by the straight bar in Fig. 1, where the statistical error is included.

Figure 2 shows the quark mass dependence of the bare values of α and β. We observe that lattice data behaves as a linear function in our quark mass region, and the chiral extrapolation to physical quark mass is carried out with a linear function of the quark mass,

$$f(\tilde{m}) = c_0 + c_1 \tilde{m}, \tag{21}$$

with $\tilde{m} = m + m_{\mathrm{res}}$, where the residual mass has been estimated as $m_{\mathrm{res}} = 0.003152(43)$ [42]. The (bare) physical quark mass has been obtained as

$$\tilde{m}_{ud}^{\mathrm{phys}} = 0.001382 \tag{22}$$

from the renormalized one $m_{ud}^{\mathrm{phys}} = -0.001770(79)$ [45].

To estimate the uncertainty due to using the linear extrapolation, we use three different fitting ranges: (i) $m \in [0.005, 0.03]$ (3.4,2.7), (ii) $m \in [0.005, 0.02]$ (2.5,1.1), and (iii) $m \in [0.01, 0.03]$ (2.5,2.5), where the numbers in the brackets show the resultant $\chi^2/\mathrm{d.o.f.}$ for α and β, respectively. The systematic error due to the assumption of linear behavior is evaluated from the maximum difference of the central values between (i) and (ii), and (i) and (iii). The results are tabulated in Table II. Compared to the previous work [32], the statistical error has been improved to 2% from 10%, and the systematic error of the chiral extrapolation is improved to 3% from 20%. Although the error estimation procedure is the same as in the previous work, because of the high statistical precision available to us the systematic error is properly estimated.

We estimate the systematic error of the lattice artifact as 5%, which is evaluated from a comparison with different lattice spacings for the hadron spectrum (see Ref. [42]). The uncertainty in the renormalization factor, which is dominated by the truncation error of the perturbative matching and running beyond the next-to-leading order. This error turns out to be the most dominant error.

The final value at $\mu = 2$ GeV in $\overline{\mathrm{MS}}$ NDR scheme (18) extrapolated to the physical quark [Eq. (22)] is

$$\alpha = -0.0144(3)(21)\ \mathrm{GeV}^3, \qquad \beta = 0.0144(3)(21)\ \mathrm{GeV}^3, \tag{23}$$

where the first error is statistical and the second is systematic (obtained in quadrature). The total error is around 15%, which is improved from 22% [32]. The superficial relation $\alpha + \beta = 0$ is accidentally observed. The relation should hold for the nonrelativistic limit and the approximate relation is known to hold at least numerically in the quenched case [30,47]. Here we have confirmed that it holds in the

TABLE III. Relative error of the systematic uncertainty in the chiral extrapolation estimated from three fitting ranges: "light" is the fitting range without the heaviest point, "heavy" is the fitting range without the lightest point, and "total" is the total one in quadrature. For reference, we also show the value of $\chi^2_{\mathrm{d.o.f.}}$ in our fitting in the "$\chi^2_{\mathrm{d.o.f.}}$" column.

	Relative error in chiral extrapolation									
Matrix element	Total	$\chi^2_{\mathrm{d.o.f.}}$	Light	$\chi^2_{\mathrm{d.o.f.}}$	Heavy	$\chi^2_{\mathrm{d.o.f.}}$	$\mathcal{O}(q^4)$	$\chi^2_{\mathrm{d.o.f.}}$	$\mathcal{O}(mq^2)$	$\chi^2_{\mathrm{d.o.f.}}$
$\langle\pi^0\vert(ud)_R u_L\vert p\rangle$	1.8%	0.6	1.6%	0.8	0.8%	0.8	0.7%	0.6	0.3%	0.2
$\langle\pi^0\vert(ud)_L u_L\vert p\rangle$	5.7%	1.4	3.8%	2.0	4.3%	1.2	2.3%	2.2	2.6%	1.9
$\langle K^0\vert(us)_R u_L\vert p\rangle$	2.8%	1.4	2.7%	1.7	0.7%	1.5	0.7%	1.6	1.1%	1.4
$\langle K^0\vert(us)_L u_L\vert p\rangle$	3.1%	1.7	0.8%	1.9	3.0%	1.7	1.0%	2.0	2.1%	0.2
$\langle K^+\vert(us)_R d_L\vert p\rangle$	3.5%	1.3	3.4%	1.5	1.0%	1.5	1.6%	1.3	2.0%	0.8
$\langle K^+\vert(us)_L d_L\vert p\rangle$	7.5%	1.6	2.3%	2.2	7.2%	1.5	3.3%	2.1	1.9%	2.7
$\langle K^+\vert(ud)_R s_L\vert p\rangle$	1.6%	0.9	1.0%	1.2	1.2%	1.1	1.3%	0.8	1.3%	0.1
$\langle K^+\vert(ud)_L s_L\vert p\rangle$	3.9%	1.7	2.1%	2.4	3.3%	1.6	1.4%	2.2	1.5%	1.7
$\langle K^+\vert(ds)_R u_L\vert p\rangle$	2.7%	1.0	2.3%	0.8	1.4%	1.1	2.3%	1.0	0.7%	0.8
$\langle K^+\vert(ds)_L u_L\vert p\rangle$	2.1%	1.8	1.5%	2.4	1.4%	1.8	0.8%	2.2	1.6%	0.8
$\langle\eta\vert(ud)_R u_L\vert p\rangle$	39.7%	1.0	31.7%	1.0	23.8%	1.4	9.4%	1.0	4.7%	1.6
$\langle\eta\vert(ud)_L u_L\vert p\rangle$	2.8%	1.0	1.3%	1.2	2.5%	1.1	1.9%	1.8	1.5%	0.7

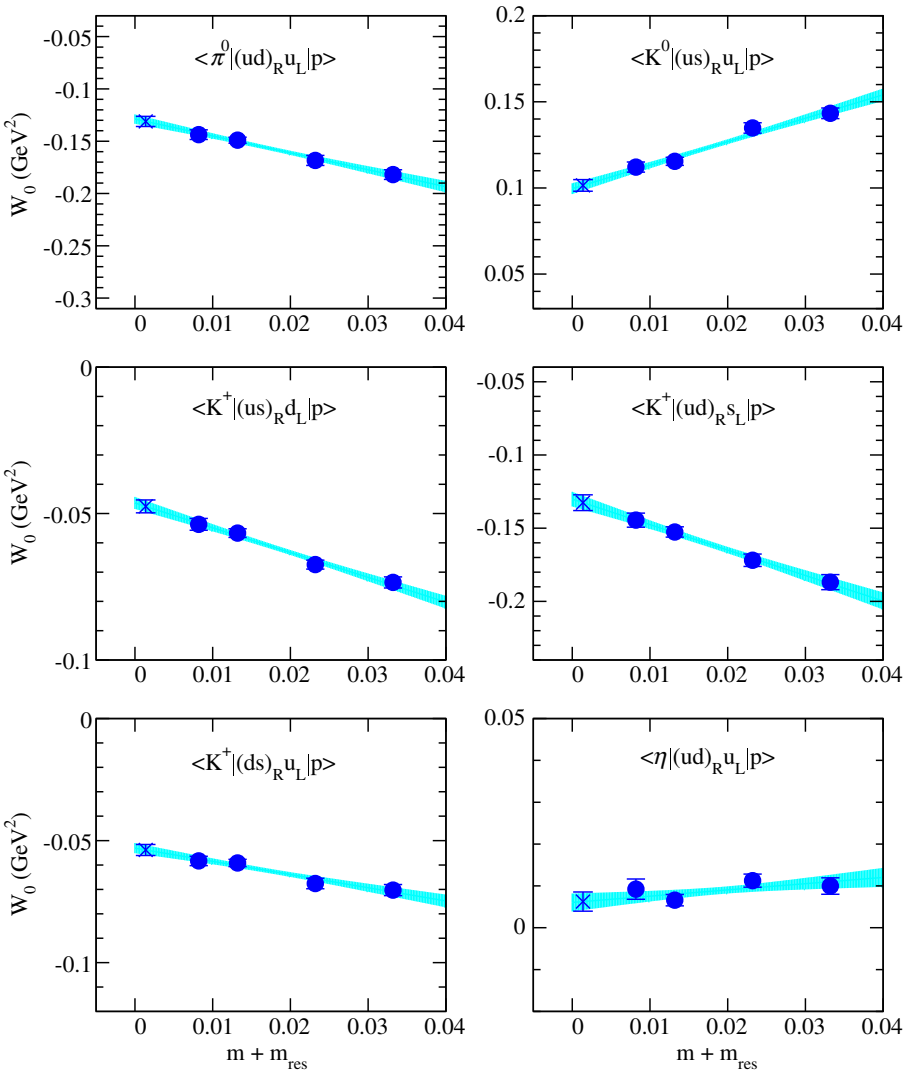

FIG. 8. Quark mass dependence of the renormalized W_0 after $q^2 = 0$ extrapolation for $\Gamma = R$ in each channel. The cross symbol denotes W_0 at the physical quark mass after linear extrapolation. The band is the extrapolation line including statistical error.

$N_f = 2 + 1$ case with an improved precision. Using these low-energy constants, the relevant form factor can be computed via the BChPT formula (see Appendix A).

V. IMPROVED RESULTS FOR THE RELEVANT FORM FACTORS

In this section, we show our improved results for the form factors from the "direct" measurement in which we compute the three-point function of $N \to P$ including the baryon-number-violating operator. Compared to our previous study [1], the results are improved by the use of the AMA technique. We also add one larger meson momentum point $n_p = (1, 1, 1)$ to the two nonzero momenta we had, $n_p = (1, 0, 0)$ and $n_p = (1, 1, 0)$. Thus, we are now able to estimate the systematic error from the $\mathcal{O}(q^4)$ term.

In Fig. 3, we plot the effective mass of the nucleon, pion, and kaon with the momentum we use in the construction of the ratio (13). One clearly sees the plateau starting from $t = 6$ in these hadrons, so from here we can see that the ground state is dominant from $t = 6$.

Figure 4—in which we plot the time-slice dependence of the matrix element extracted from the ratio (13) for the $p \to \pi^0$ mode at our lightest point $m = 0.005$—shows the comparison with two different source-sink separations, $t_s = 18$ and 22, corresponding to $t_s = 1.98$ and 2.43 fm, respectively. The time separation $t_s = 18$ is new in this study and is four-time slices shorter than the original $t_s = 22$ [1]. We observe a plateau for shorter separation at $t \in [12, 16]$, where the denominators are also dominated by the ground state (see Fig. 3 and note that the source is located at $t = 5$ here). The plateaus from two separations are consistent and the shorter separation yields significantly better statistical accuracy. Let us note that the clear plateau is observed even in the largest momentum case $n_p = (1, 1, 1)$. Hereafter, we only use the result with $t_s = 18$, and further test the effect of excited-state contamination by changing the fitting range below.

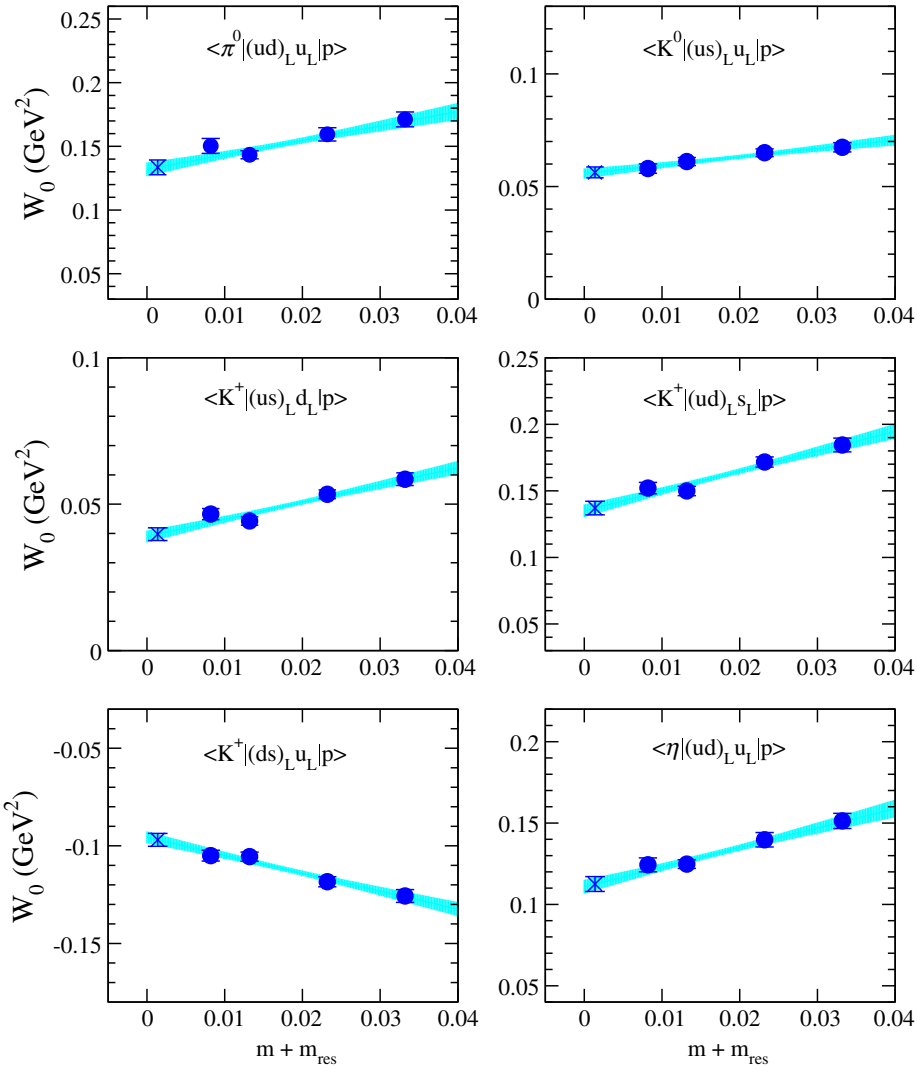

FIG. 9. Quark mass dependence of the renormalized W_0 after $q^2 = 0$ extrapolation for $\Gamma = L$. Each symbol is the same as in Fig. 8.

Figure 5 shows the result of the plateau fit for W_0 using the fitting ranges $t \in [11, 17]$ and $t \in [12, 16]$ to study the effect of excited-state contamination on the signal. We observe that these values are consistent within 1 sigma error in each q^2, while the central value has slight tension, especially for the lowest momentum in $\Gamma = L$. In order to estimate the systematic uncertainties including the effect of excited-state contamination, we compare the results using these fitting ranges. Such a comparison will be discussed later.

A. Global fitting

To perform the extrapolation to the kinematic point and physical pion mass simultaneously, we globally fit all lattice data with the linear ansatz for the quark mass and q^2 dependence as

$$F_{W_0} = A_0 + A_1\tilde{m} + A_2 q^2, \tag{24}$$

where $\tilde{m}$ has the same definition as in Eq. (21). Figures 6 and 7 plot the renormalized $W_0(q^2)$ for every decay channel and for each quark mass. We observe that lattice data for each quark mass (which are denoted by the same symbols in Figs. 6 and 7) has a linear q^2 dependence. For the mass dependence, we also observe a monotonic decrease or increase when m is increasing. Even when using the linear ansatz, χ^2/d.o.f. is reasonably small (note that we use uncorrelated fits), as presented in the first "$\chi^2_{\text{d.o.f.}}$" column of Table III.

We next study the uncertainties in the fitting related with the mass dependence, following the method used in Ref. [1]. The estimated errors are attributed to the higher-order correction than $\mathcal{O}(m)$ and a part (at least) of the finite-volume effect. Table III presents the errors estimated with the discrepancy from the central value, which is obtained in the full range $m \in [0.005, 0.03]$ and two fitting ranges: $m \in [0.005, 0.02]$ for the "light" region and $m \in [0.01, 0.03]$ for the "heavy" region. The error with

TABLE IV. Table of the renormalized W_0 in the physical kinematics at 2 GeV in the $\overline{\text{MS}}$ NDR scheme. The fourth column contains the relative error of the systematic uncertainties. "χ" comes from the chiral extrapolation given from three different fitting ranges as explained in the text. The "q^4" and "a^2" columns are the uncertainties of the higher-order correction than $\mathcal{O}(q^2)$ and the lattice artifact at $\mathcal{O}(a^2)$, respectively. The "m_s" column is the uncertainty coming from using the unphysical strange quark mass. Δ_Z and Δ_a are the errors of the renormalization factor and lattice scale estimate, respectively.

				Systematic error [%]						
Matrix element	W_0 GeV^2	Statistical[%]	Total	χ	q^4	mq^2	a^2	m_s	Δ_a	Δ_Z
$\langle\pi^0\vert(ud)_R u_L\vert p\rangle$	−0.131(4)(13)	3.0	9.7	1.8	0.7	0.3	5.0	⋯	0.6	8.1
$\langle\pi^0\vert(ud)_L u_L\vert p\rangle$	0.134(5)(16)	3.4	11.6	5.7	2.3	2.6				
$\langle\pi^+\vert(du)_R d_L\vert p\rangle$	−0.186(6)(18)	3.0	9.7	1.8	0.7	0.3				
$\langle\pi^+\vert(du)_L d_L\vert p\rangle$	0.189(6)(22)	3.4	11.6	5.7	2.3	2.6				
$\langle K^0\vert(us)_R u_L\vert p\rangle$	0.103(3)(11)	2.8	10.4	2.8	0.7	1.1	5.0	3.0	0.6	8.1
$\langle K^0\vert(us)_L u_L\vert p\rangle$	0.057(2)(6)	3.5	10.7	3.1	1.0	2.1				
$\langle K^+\vert(us)_R d_L\vert p\rangle$	−0.049(2)(5)	3.7	10.9	3.5	1.6	2.0				
$\langle K^+\vert(us)_L d_L\vert p\rangle$	0.041(2)(5)	4.4	13.1	7.5	3.3	1.9				
$\langle K^+\vert(ud)_R s_L\vert p\rangle$	−0.134(4)(14)	3.2	10.3	1.6	1.3	1.3				
$\langle K^+\vert(ud)_L s_L\vert p\rangle$	0.139(4)(15)	3.0	10.9	3.9	1.4	1.5				
$\langle K^+\vert(ds)_R u_L\vert p\rangle$	−0.054(2)(6)	3.6	10.6	2.7	2.3	0.7				
$\langle K^+\vert(ds)_L u_L\vert p\rangle$	−0.098(3)(10)	2.8	10.3	2.1	0.8	1.6				
$\langle\eta\vert(ud)_R u_L\vert p\rangle$	0.006(2)(3)	30.0	42.1	39.7	9.4	4.7	5.0	⋯	0.6	8.1
$\langle\eta\vert(ud)_L u_L\vert p\rangle$	0.113(3)(12)	3.1	10.2	2.8	1.9	1.5				

the "light" region can be an estimate of the $\mathcal{O}(m^2)$ correction since the exclusion of the heavy mass makes a correction less than $\mathcal{O}(m^2)$. On the other hand, the error with the "heavy" region can (at least partly) be due to the finite-volume effect, since the lightest point suffers most from the effect with the fixed volume. In each range, χ^2/d.o.f. is not significantly large. The values presented in the table are taken as the maximum error compared with the result obtained in two t fitting ranges $t \in [12, 16]$ and $t \in [11, 17]$. The "total" error of the chiral extrapolation in the table is calculated by adding the two errors ("light" and "heavy") in quadrature.

In a similar manner as the "light" error, the $\mathcal{O}(q^4)$ error is estimated from the difference of the results obtained with the full range of q^2 with all of the nonzero meson momenta and the shorter range where the largest $|q^2|$ ($n_p = (1, 1, 1)$) is neglected. The result is shown in the column labeled "$\mathcal{O}(q^4)$" in Table III. This error turns out to be smaller than that of the "chiral" extrapolation.

As shown in Figs. 6 and 7, the q^2 dependence obtained by extrapolating the data in the "direct" method does not largely differ from BChPT including α and β obtained in Sec. IV, especially the fact that the $p \to \pi$ channels have a tendency to be close to each other with increasing $q^2 > 0$. There is a discrepancy up to about a factor of 2 around the kinematics point. Such a comparison will be discussed later.

B. Sequential fitting

In the global fitting we estimated a part of the systematic errors due to omitting the higher-order terms in the expansion of the light quark mass $\tilde{m}$ and squared momentum transfer q^2. Those estimated are of $\mathcal{O}(\tilde{m}^2)$ and $\mathcal{O}(q^4)$. The remaining error is of $\mathcal{O}(\tilde{m}q^2)$. For the estimate we use the same method as in Ref. [1]. The procedure is that first the $q^2 \to 0$ extrapolation is carried out for each fixed quark mass with a linear function; then, the chiral extrapolation is performed (see Figs. 8 and 9). By doing this we are taking into account the q^2 dependence in the prefactor of the linear quark mass term A_1 in Eq. (24). If the result is different, it is attributed as the m effect in A_1, and thus is of $\mathcal{O}(\tilde{m}q^2)$. The last column of Table III shows the χ^2 per degree of freedom for the final $\tilde{m}$ linear fit. The second to last column represents the systematic error estimated in this analysis. It turns out to be subdominant in the fitting errors.

C. The final results

Table IV presents a summary of the nucleon decay form factors for each operator and final state with the statistical and systematic errors. The statistical error is significantly reduced to 1/4–1/6 from our previous study [1] and now is subdominant. The systematic errors for the extrapolation discussed above are combined and shown in the

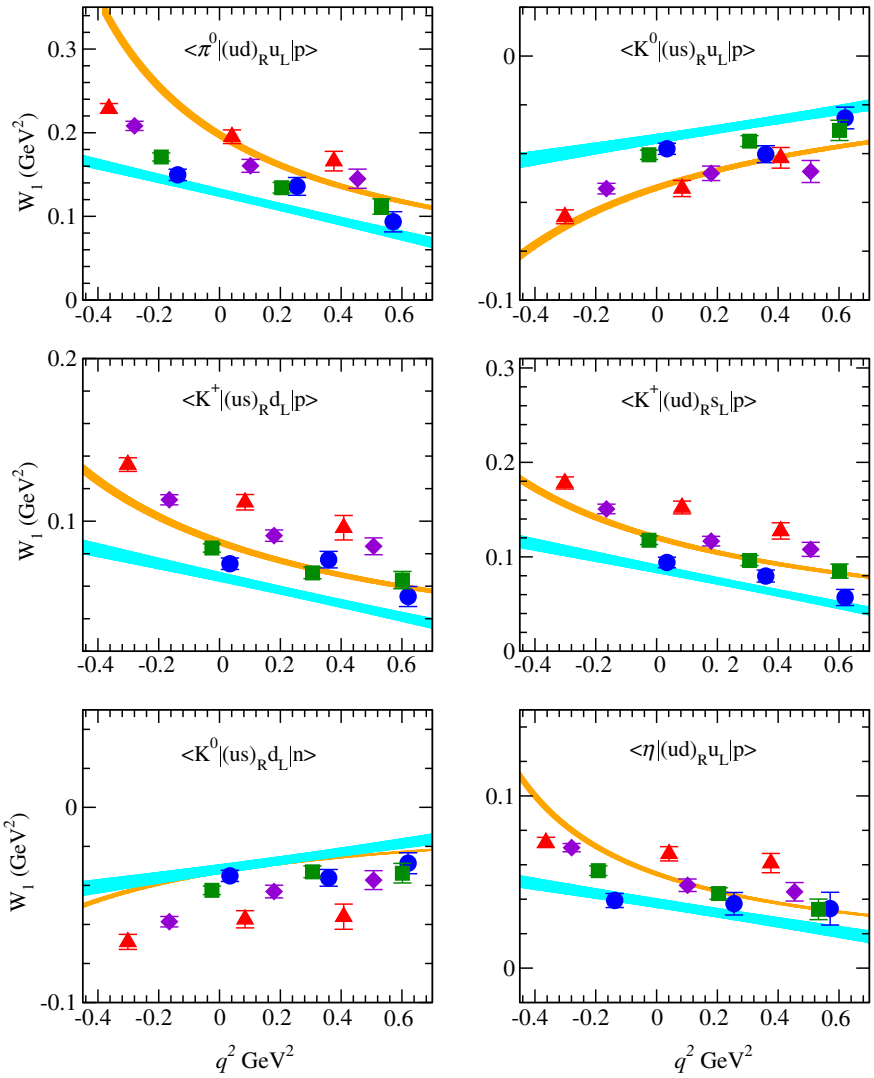

FIG. 10. Renormalized W_1 for $\Gamma = R$. Each symbol is the same as in Fig. 6.

"$(\tilde{m}q^2)$-fit" column. Since we use a single lattice cutoff in this study, the lattice artifact, which is a $\mathcal{O}(a^2)$ correction, is estimated from the scaling study of the hadron spectrum, as done in Ref. [42]. The mass of the valence strange quark which participates in the matrix elements of the kaon final state is set equal to its sea-quark mass, $m = 0.04$. There is a mismatch with the physical strange mass. The associated systematic error is estimated using a subset of the $m = 0.005$ ensemble by setting $m = 0.343$.[4] The difference with regards to the central value is 3% at most. We conservatively take 3% as the systematic error of the form factors for the process with the kaon final state due to the use of the mismatched strange sea and valence quark masses. On the other hand, the mismatch effect of the strange sea quark is expected to be much less than that of the valence quark; thus, it is negligible in the pion and eta final states. The largest uncertainty comes from that of the renormalization factor, which is dominated by the systematic error due to the truncation of the perturbative matching [Eq. (18)]. The total error (summed in quadrature) amounts to 10–15% for the form factors with a pion or kaon final state.

Additionally, Table V presents the matrix element with a muon final state, $m_l = m_\mu$. W_μ in Eq. (3) is made from two form factors: W_0 and W_1. As seen in Figs. 10 and 11, the magnitude of W_1 in each matrix element is similar to W_0, and hence the W_1 term multiplied by the factor $m_\mu/m_N \sim 0.1$ in W_μ has a roughly 10% effect on the matrix element in the kinematics with a muon final state.

Note that for the matrix element with an eta final state we are ignoring the disconnected diagram, which means there remains additional uncertainty. However, the contribution from the disconnected diagram is expected to be small due to Okubo-Zweig-Iizuka suppression. A detailed study of

[4]The value comes from the physical strange quark mass used in the previous study. The latest estimate of the physical strange mass [45] turns out to be 0.03224, which is not large enough to change the systematic error estimate.

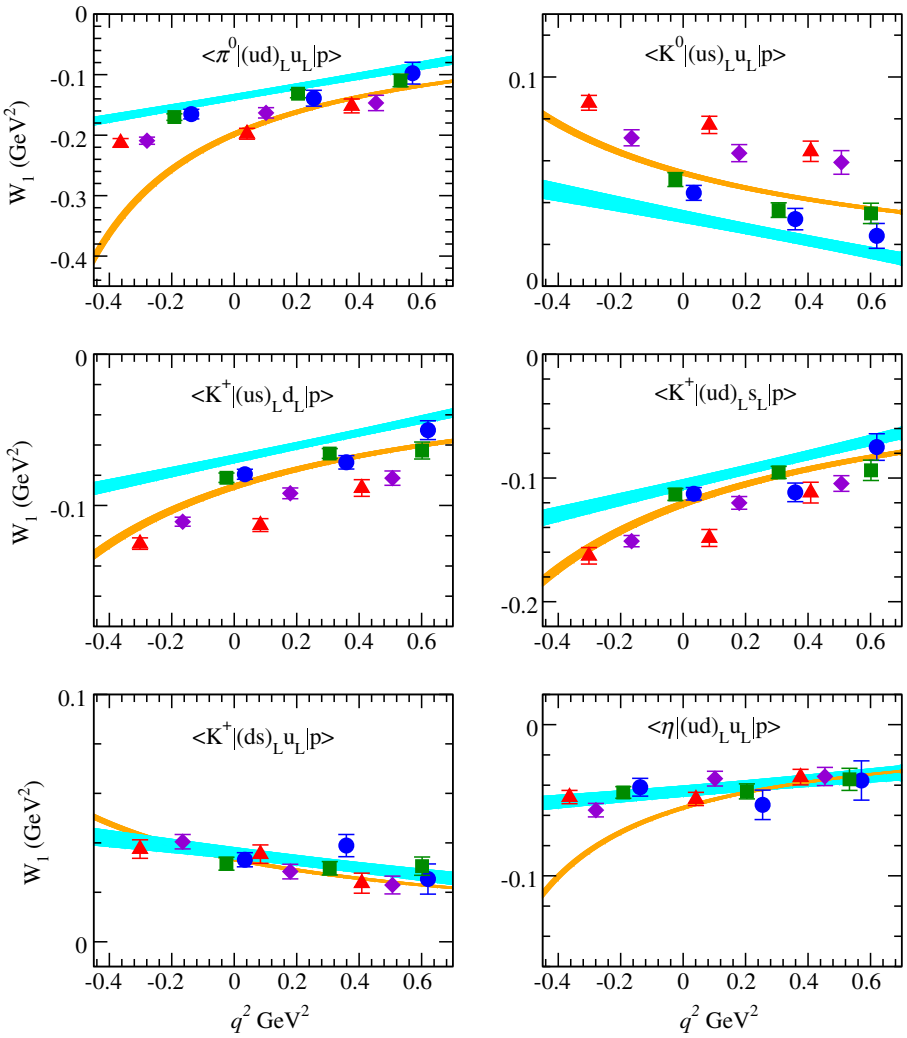

FIG. 11. Renormalized W_1 for $\Gamma = L$. Each symbol is the same as in Fig. 6.

the eta sector including the disconnected diagram is beyond the scope of this paper.

All of the final results for the relevant form factors of proton decay W_0 and W_μ with the "direct" method are summarized in Fig. 12. The results are also compared with those with the "indirect" method through BChPT using lattice LECs (denoted as $W_0^{\alpha,\beta}$ and $W_\mu^{\alpha,\beta}$). The "indirect" method always overestimates the form factor. The amount is 25% or more except for two cases ($\langle K^+|(us)_{R/L}d_L|p\rangle$). In contrast to the previous study [1], each error becomes a lot smaller, and now we clearly see the discrepancy between $W_{0,\mu}$ and $W_{0,\mu}^{\alpha,\beta}$ for most cases.

TABLE V. Table of the renormalized W_μ [Eq. (3)], which is the form factor in the physical kinematics with a final state of μ^+.

Matrix element	W_μ GeV^2
$\langle\pi^0\|(ud)_R u_L\|p\rangle$	−0.118(3)(12)
$\langle\pi^0\|(ud)_L u_L\|p\rangle$	0.119(4)(14)
$\langle\pi^-\|(du)_R u_L\|n\rangle$	−0.167(4)(16)
$\langle\pi^-\|(du)_L u_L\|n\rangle$	0.169(5)(20)
$\langle K^0\|(us)_R u_L\|p\rangle$	0.099(2)(10)
$\langle K^0\|(us)_L u_L\|p\rangle$	0.061(2)(7)
$\langle\eta\|(ud)_R u_L\|p\rangle$	0.011(2)(3)
$\langle\eta\|(ud)_L u_L\|p\rangle$	0.108(3)(11)

The fact that the indirect method (which uses BChPT) works poorly is understandable, as the physical kinematical point for the outgoing pion is far from the soft pion limit, where the ChPT description becomes arbitrarily precise. We tested the soft pion theorem for the form factors of the pion final state, which are found in Appendix B. There, the results from the indirect and direct methods appear to be consistent with each other in the soft pion limit.

VI. APPLICATION TO THE KINEMATICS OF A DARK MATTER MODEL

In this section, we present some interesting applications of the model using other kinematics, in which an energetic

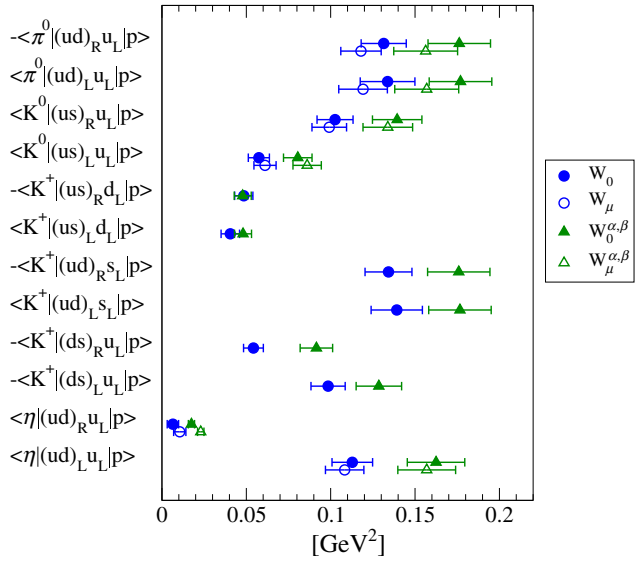

FIG. 12. Summary of the matrix elements obtained in our study. "W_0, W_μ" are evaluated with the "direct" method, and "$W_0^{\alpha,\beta}$, $W_\mu^{\alpha,\beta}$" are evaluated with the "indirect" method, including the systematic error as discussed in the text.

pion is emitted from a proton and dark matter (DM) appears instead of a lepton. According to Refs. [36,37], the so-called "induced nucleon decay (IND)" scenario, the proton should decay to DM particles (Ψ, Φ) having the antibaryon number with mass $m_{\Phi,\Psi} \sim 2$–3 GeV. This model, motivated by the hypothesis of an asymmetric DM model [48], assumes that the net baryon number in the Universe is symmetric, in which the SM particle sector has a baryon number asymmetry while the particle X_1 in the hidden sector has the opposite asymmetry, and DM (Ψ, Φ) has been generated from X_1 decay in the early Universe. If it is consistent with the Sakharov conditions, such decay should have baryon number violation and CP violation in non-thermal circumstances. In the IND model, the nucleon and pseudoscalar are interacting with DM through X_1, and thus the scattering processes $\Psi N \to \Phi^\dagger P$ and $\Phi N \to \bar{\Psi} P$ occur. The interesting feature of this model is that the QCD matrix element is the same as that of the standard nucleon decay, since the operator related to DM scattering is composed of an effective three-quark interaction,

$$u_R d_R d_R \Psi_R \Phi / \Lambda^3 + \text{H.c.}, \tag{25}$$

and the only difference is its kinematics of which q^2 is different from the on-shell lepton. In principle, the lattice calculation is accessible to the matrix element at q^2 values relevant to this model, and thus we can also provide a more accurate value for the prediction of this model.

The DM mass $m_{\Phi,\Psi} \sim 2$–3 GeV is predicted from cosmological observations and DM stability, which is much heavier than the lepton mass, so that under momentum conservation the pion has finite momentum, which is shifted to the region $-q^2 < 0$ (to the right of zero in Figs. 6, 7, 10, and 11). Recalling the formula for the transition form factor in Eq. (2), the relevant form factors are both W_0 and W_1, since the DM mass is heavy, $q^2 \sim 4m_{\Phi,\Psi}^2 > m_p^2$. A typical meson momentum in the IND model is $|\vec{p}| = 1$ GeV, in which the kinematics of the IND model is $q^2 \simeq 1$ GeV^2. Figure 13 plots $W_{0,1}$ and $W_{0,1}^{\alpha,\beta}$ extrapolated to $q^2 = 1$ GeV^2 using lattice results. Focusing on the pion channel, one sees that the "direct" lattice calculation provides 25–50% of the value of $W_{0,1}^{\alpha,\beta}$ used for the estimate of the proton lifetime in the IND model [36,37]. Concerning the convergence issue of BChPT at tree level applied to energetic mesons arising in this kinematics, our lattice result indicates such a difference from an evaluation based on tree-level BChPT may not be negligible. One sees

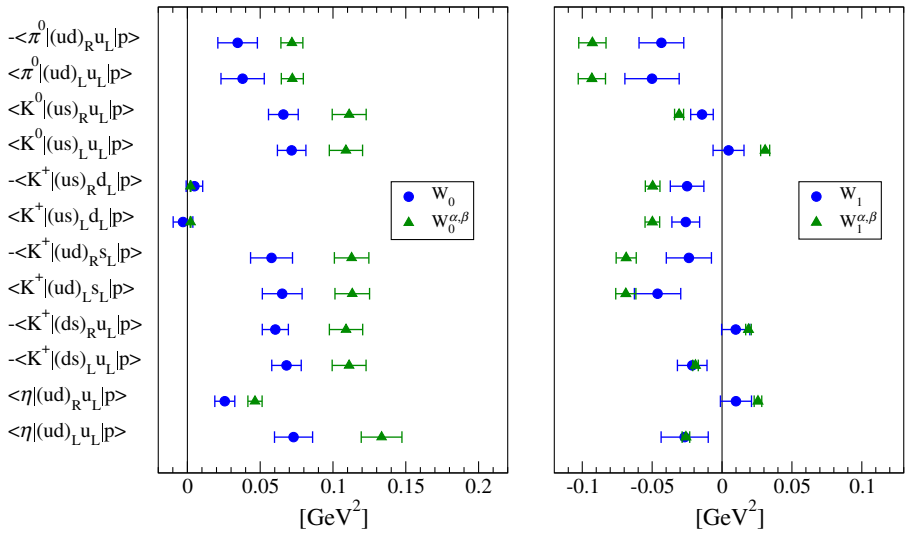

FIG. 13. Summary of the matrix elements "$W_{0,1}$, $W_{0,1}^{\alpha,\beta}$" for a typical meson momentum $|\vec{p}| = 1$ GeV for the IND model.

TABLE VI. Comparison of the matrix element calculations in lattice QCD from $N_f = 0$ to $N_f = 3$ with several groups. The errors of α, β, and W_0 are the total error, which is combined with the statistical and systematic errors in quadrature. We remark that * denotes the results obtained using renormalization constants with perturbative matching factors that have an error, as explained in the text. With the error corrected the values would increase by as much as ∼7%.

Ref.	JLQCD (2000) [29]	CP-PACS & JLQCD (2004) [31]	RBC (2007) [30]	QCDSF (2008) [46]	RBC/UKQCD (2008,2014) [1,32]	This work
Fermion	Wilson	Wilson	DW	Wilson	DW	DW
N_f	0	0	0 and 2	2	3	3
Volume (fm^3)	$(2.4)^2 \times 4.1$	$(3.3)^3$	Quench $(1.6)^3$ Two-flavor $(1.9)^3$	$(1.68)^3$	$(2.65)^3$	$(2.65)^3$
a (fm)	0.09	0	Quench 0.1 Two-flavor 0.12	0.07	0.11	0.11
m_π (GeV)	0.45–0.73	0.6–1.2	Quench 0.39–0.58 Two-flavor 0.48–0.67	0.42–1.18	0.34–0.69	0.34–0.69
Renorm. μ	One-loop $1/a$, π/a	One-loop 2 GeV	NPR 2 GeV	NPR 2 GeV	NPR 2 GeV	NPR 2 GeV
α (GeV^3)	−0.015(1)	$-0.0090(^{+10}_{-21})$	Quench $-0.0100^*(19)$ Two-flavor $-0.0118^*(21)$	−0.0091(4)	$-0.0119^*(26)$	−0.0144(15)
β (GeV^3)	0.014(1)	$0.0096(^{+11}_{-22})$	Quench $0.0108^*(21)$ Two-flavor $0.0118^*(21)$	0.0090(4)	$0.0128^*(28)$	0.0144(15)
$p \to \pi^0$						
W_0^{LR} (GeV^2)	−0.134(16)	⋯	Quench $-0.060^*(18)$ Two-flavor ⋯	⋯	$-0.103^*(41)$	−0.131(13)
W_0^{LL} (GeV^2)	0.128(17)	⋯	Quench $0.086^*(22)$ Two-flavor	⋯	$0.133^*(40)$	0.134(16)

that a possible effect on the proton decay amplitude when using $W_{0,1}$ in our results may be a factor of 4 or greater suppression compared with the results obtained with BChPT. This potentially large systematic error needs to be considered when one uses BChPT for this purpose.

VII. SUMMARY AND DISCUSSION

In this paper we presented an improved computation of the proton decay matrix element using the all-mode-averaging technique on $N_f = 2 + 1$ domain-wall fermion configurations. Compared to previous work [1] (also see Table VI), the statistical error has been significantly reduced for both the low-energy constant in BChPT and the matrix element extracted from the three-point function. Our analysis using the precise lattice data with three different momenta, by which we add one more higher q^2, can evaluate a higher-order correction than $\mathcal{O}(q^2)$. The systematic uncertainty for the chiral extrapolation due to using the unphysical pion around $m_\pi = 0.33$ GeV is still larger than the $\mathcal{O}(q^4)$ and $\mathcal{O}(mq^2)$ corrections, while its magnitude strongly depends on the chirality of the baryon-number-violating operator. This uncertainty can be reduced in future work by using a larger volume than 3 fm^3 for the physical pion mass generated by the RBC-UKQCD Collaboration [45]. Currently, the dominant errors come from the uncertainties of the renormalization factor and lattice artifact correction, and those may be reduced by further efforts using the renormalization scheme and a comparison with finer lattices [45]. The final result of $W_{0,\mu}$ is presented in Tables IV and V, in which the total error in the pion channel for the e, ν, and μ final states is 10–14%,

and that of the kaon sector is of a similar precision. Compared to $W_{0,\mu}^{\alpha,\beta}$ via the "indirect" method using the improved lattice calculation of LECs, $W_{0,\mu}$ from the "direct" method is 1.3–1.4 times smaller for the proton decay amplitude. This means that if our result for $W_{0,\mu}$ is incorporated into a GUT model prediction instead of $W_{0,\mu}^{\alpha,\beta}$, the proton lifetime prediction may become about 2 times larger. Finally, we noted that our calculation is also applicable to the other kinematics corresponding to a dark matter model, and pointed out that there will be a higher-order correction than next-to-leading-order BChPT. Our lattice calculation of $W_{0,\mu}$ can provide a more reliable value for such a model.

ACKNOWLEDGMENTS

We thank members of RIKEN-BNL-Columbia (RBC) and the UKQCD Collaboration for sharing USQCD resources for part of our calculation. E. S. thanks Hooman Davoudiasl for a useful discussion. Numerical calculations were performed using the RICC at RIKEN and the Ds cluster at FNAL. This work was supported by the JSPS KAKENHI Grants No. JP22540301 (T. I.), No. JP22224003 (Y. A.), No. JP16K05320 (Y. A.), MEXT KAKENHI Grants No. JP23105714 (E. S.), No. JP23105715 (T. I.), and U.S. DOE Grant No. DE-SC0012704 (T. I. and A. S.). We are grateful to BNL, the RIKEN BNL Research Center, RIKEN Advanced Center for Computing and Communication (ACCC), and USQCD for providing resources necessary for completion of this work. E. S. also thanks the INT and organizers of Program INT-15-3 "Intersections of BSM Phenomenology and QCD for New Physics Searches," September 14–October 23, 2015, and Ryuichiro Kitano for his support from MEXT Grant-in-Aid for Scientific Research on Innovative Areas (No. JP25105011).

APPENDIX A: LEADING FORMULA FOR THE PROTON DECAY MATRIX ELEMENT IN BCHPT

According to BChPT [25,29], the relevant matrix element, $W_0^{\alpha,\beta}$, can be represented as

$$\langle \pi^0|(ud)_R u_L|p\rangle = \frac{\alpha}{\sqrt{2}f}(1+D+F), \tag{A1}$$

$$\langle \pi^0|(ud)_L u_L|p\rangle = \frac{\beta}{\sqrt{2}f}(1+D+F), \tag{A2}$$

$$\langle K^0|(us)_R u_L|p\rangle = -\frac{\alpha}{f}\left(1+(D-F)\frac{m_N}{m_B}\right), \tag{A3}$$

$$\langle K^0|(us)_L u_L|p\rangle = \frac{\beta}{f}\left(1-(D-F)\frac{m_N}{m_B}\right), \tag{A4}$$

$$\langle K^+|(us)_R d_L|p\rangle = \frac{\alpha}{f}\frac{2D}{3}\frac{m_N}{m_B}, \tag{A5}$$

$$\langle K^+|(us)_L d_L|p\rangle = \frac{\beta}{f}\frac{2D}{3}\frac{m_N}{m_B}, \tag{A6}$$

$$\langle K^+|(ud)_R s_L|p\rangle = \frac{\alpha}{f}\left(1+\left(\frac{D}{3}+F\right)\frac{m_N}{m_B}\right), \tag{A7}$$

$$\langle K^+|(ud)_L s_L|p\rangle = \frac{\beta}{f}\left(1+\left(\frac{D}{3}+F\right)\frac{m_N}{m_B}\right), \tag{A8}$$

$$\langle K^+|(ds)_R u_L|p\rangle = \frac{\alpha}{f}\left(1+\left(\frac{D}{3}-F\right)\frac{m_N}{m_B}\right), \tag{A9}$$

$$\langle K^+|(ds)_L u_L|p\rangle = -\frac{\beta}{f}\left(1-\left(\frac{D}{3}-F\right)\frac{m_N}{m_B}\right), \tag{A10}$$

$$\langle \eta|(ud)_R u_L|p\rangle = -\frac{\alpha}{\sqrt{6}f}(1+D-3F), \tag{A11}$$

$$\langle \eta|(ud)_L u_L|p\rangle = \frac{\beta}{\sqrt{6}f}(3-D+3F), \tag{A12}$$

with the low-energy parameters $D = 0.80$ and $F = 0.47$. In this paper, we use $f = 0.131$ GeV, $m_N = 0.94$ GeV, and $m_B = 1.15$ GeV [32].

APPENDIX B: TEST OF THE SOFT-PION THEOREM

In this appendix, we present the analysis of the matrix element in the soft-pion limit. In this limit, each matrix element is described in terms of the leading order of BChPT. In order to test that the lattice calculation has a value that is consistent with BChPT in the soft-pion limit, we calculate the matrix element win two ways: one is BChPT using LECs α and β obtained by "indirect" lattice calculation, and the second is the matrix element obtained by "direct" lattice calculation. Using LECs the matrix element is

$$\begin{aligned}\langle \pi^0|(ud)_R u_L|p\rangle_{sp} &= \frac{\alpha}{\sqrt{2}f_0}P_L u_N,\\ \langle \pi^0|(ud)_L u_L|p\rangle_{sp} &= \frac{\beta}{\sqrt{2}f_0}P_L u_N,\end{aligned} \tag{B1}$$

with the subscript sp denoting the soft-pion limit, which corresponds to $p_\mu \to 0$ and the chiral limit. On the other hand, the left-hand side of the above equation is also represented as

$$\langle \pi^0|(ud)_\Gamma u_L|p\rangle_{sp} = P_L W_{sp} u_N, \tag{B2}$$

in which W_{sp} is obtained from the form factor at $\vec{p} = (0,0,0)$ for Eq. (2) in the chiral limit. We define such a form factor as

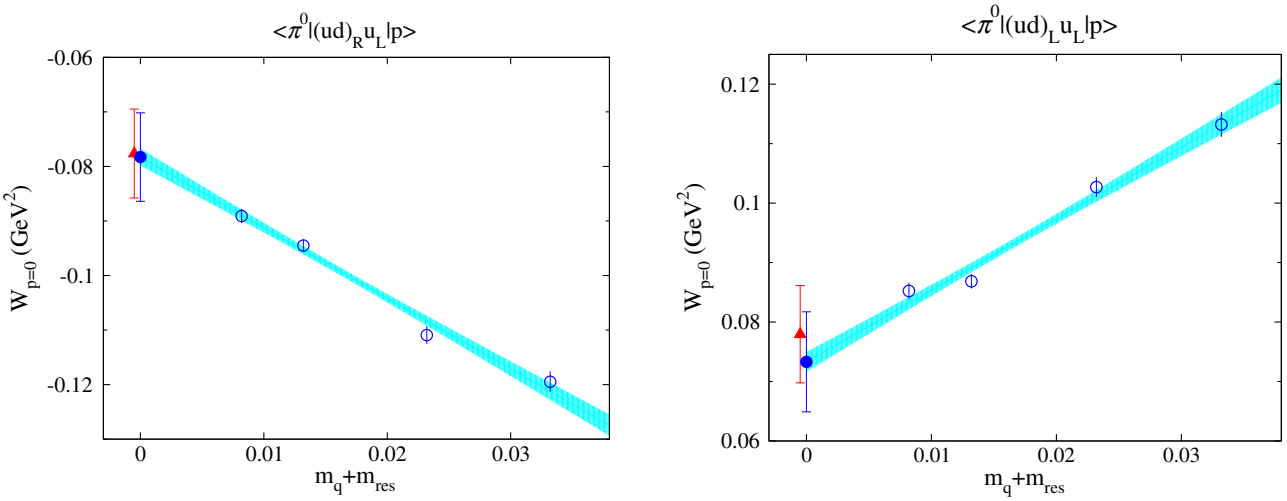

FIG. 14. The open circles denote the lattice results for $W_{\vec{p}=0}$ for RL (left) and LL (right) chirality for each quark mass, and the colored band shows the fitting function with the statistical error. In the chiral limit, the triangle and filled circle denote the value of BChPT and the extrapolated result in the soft-pion limit, respectively. The error bars denote the total error including the systematic one, which is obtained by the same procedure as in Sec. V.

$$W_{\vec{p}=0} = \lim_{t_1-t,t-t_0\to\infty} R_3^{\Gamma}(t,t_1,t_0;0,P_4), \tag{B3}$$

and we take the extrapolation to zero quark mass with the linear ansatz

$$W_{\vec{p}=0} = W_{sp} + c_1\tilde{m}. \tag{B4}$$

The linear ansatz assumes a negligibly small $\sqrt{\tilde{m}} \sim m_\pi$ term even for $\tilde{m} \simeq 0$.

Figure 14 shows the lattice results for $W_{\vec{p}=0}$ and W_{sp}. We also show the lines of chiral extrapolation and the extrapolated values with the linear ansatz in the chiral limit. Here we estimate the systematic uncertainties due to chiral extrapolation by comparing the "light" and "heavy" regions, as well as in Table III. We also add the uncertainties of the renormalization factor and lattice artifact, as in Table IV. One sees that the lattice data is close to a linear function and the extrapolated value is consistent with BChPT within 1 sigma error. We notice that there is no visible curvature of the square root of the quark mass. It indicates that the coefficient of the square root of the quark mass may not be significantly large.

[1] Y. Aoki, E. Shintani, and A. Soni, Phys. Rev. D **89**, 014505 (2014).
[2] H. Nishino *et al.* (Super-Kamiokande Collaboration), Phys. Rev. Lett. **102**, 141801 (2009).
[3] K. Babu *et al.*, arXiv:1311.5285.
[4] K. Abe *et al.* (Super-Kamiokande Collaboration), Phys. Rev. D **90**, 072005 (2014).
[5] E. Kearns *et al.* (Hyper-Kamiokande Working Group Collaboration), arXiv:1309.0184.
[6] A. Martin and G. C. Stavenga, Phys. Rev. D **85**, 095010 (2012).
[7] N. Maekawa and Y. Muramatsu, Phys. Rev. D **88**, 095008 (2013).
[8] N. Maekawa and Y. Muramatsu, Prog. Theor. Exp. Phys. **2014**, 113B03 (2014).
[9] A. de Gouvea, J. Herrero-Garcia, and A. Kobach, Phys. Rev. D **90**, 016011 (2014).
[10] J. L. Evans, N. Nagata, and K. A. Olive, Phys. Rev. D **91**, 055027 (2015).
[11] Y. Mambrini, N. Nagata, K. A. Olive, J. Quevillon, and J. Zheng, Phys. Rev. D **91**, 095010 (2015).
[12] R. Huo, S. Matsumoto, Y.-L. Sming Tsai, and T. T. Yanagida, J. High Energy Phys. 09 (2016) 162.
[13] B. Bajc, S. Lavignac, and T. Mede, J. High Energy Phys. 01 (2016) 044.
[14] J. Ellis, J. L. Evans, F. Luo, N. Nagata, K. A. Olive, and P. Sandick, Eur. Phys. J. C **76**, 8 (2016).
[15] T. D. Brennan, Phys. Rev. D **95**, 065008 (2017).
[16] J. Hisano, T. Kuwahara, and Y. Omura, Nucl. Phys. **B898**, 1 (2015); **B907**, 476(E) (2016).
[17] P. F. Perez and C. Murgui, Phys. Rev. D **94**, 075014 (2016).
[18] B. Bajc, J. Hisano, T. Kuwahara, and Y. Omura, Nucl. Phys. **B910**, 1 (2016).

[19] J. Ellis, J. L. Evans, A. Mustafayev, N. Nagata, and K. A. Olive, Eur. Phys. J. C **76**, 592 (2016).
[20] K. S. Babu, B. Bajc, and S. Saad, Phys. Rev. D **94**, 015030 (2016).
[21] K. S. Babu, B. Bajc, and S. Saad, J. High Energy Phys. 02 (2017) 136.
[22] H. Koleov and M. Malinsk, arXiv:1612.09178.
[23] P. Cox, A. Kusenko, O. Sumensari, and T. T. Yanagida, J. High Energy Phys. 03 (2017) 035.
[24] K. Harigaya, T. Lin, and H. K. Lou, J. High Energy Phys. 09 (2016) 014.
[25] M. Claudson, M. B. Wise, and L. J. Hall, Nucl. Phys. **B195**, 297 (1982).
[26] Y. Hara, S. Itoh, Y. Iwasaki, and T. Yoshie, Phys. Rev. D **34**, 3399 (1986).
[27] K. C. Bowler, D. Daniel, T. D. Kieu, D. G. Richards, and C. J. Scott, Nucl. Phys. **B296**, 431 (1988).
[28] M. B. Gavela, S. F. King, C. T. Sachrajda, G. Martinelli, M. L. Paciello, and B. Taglienti, Nucl. Phys. **B312**, 269 (1989).
[29] S. Aoki *et al.* (JLQCD Collaboration), Phys. Rev. D **62**, 014506 (2000).
[30] Y. Aoki, C. Dawson, J. Noaki, and A. Soni, Phys. Rev. D **75**, 014507 (2007).
[31] N. Tsutsui *et al.* (CP-PACS Collaboration), Phys. Rev. D **70**, 111501 (2004).
[32] Y. Aoki, P. Boyle, P. Cooney, L. Del Debbio, R. Kenway, C. M. Maynard, A. Soni, and R. Tweedie (RBC and UKQCD Collaborations), Phys. Rev. D **78**, 054505 (2008).
[33] T. Blum, T. Izubuchi, and E. Shintani, Phys. Rev. D **88**, 094503 (2013).
[34] T. Blum, T. Izubuchi, and E. Shintani, Proc. Sci., LATTICE2012 (**2012**) 262, arXiv:1212.5542.
[35] E. Shintani, R. Arthur, T. Blum, T. Izubuchi, C. Jung, and C. Lehner, Phys. Rev. D **91**, 114511 (2015).
[36] H. Davoudiasl, D. E. Morrissey, K. Sigurdson, and S. Tulin, Phys. Rev. Lett. **105**, 211304 (2010).
[37] H. Davoudiasl, D. E. Morrissey, K. Sigurdson, and S. Tulin, Phys. Rev. D **84**, 096008 (2011).
[38] H. Davoudiasl, Phys. Rev. Lett. **114**, 051802 (2015).
[39] S. Weinberg, Phys. Rev. Lett. **43**, 1566 (1979).
[40] F. Wilczek and A. Zee, Phys. Rev. Lett. **43**, 1571 (1979).
[41] L. F. Abbott and M. B. Wise, Phys. Rev. D **22**, 2208 (1980).
[42] Y. Aoki *et al.* (RBC and UKQCD Collaborations), Phys. Rev. D **83**, 074508 (2011).
[43] G. von Hippel, T. D. Rae, E. Shintani, and H. Wittig, Nucl. Phys. **B914**, 138 (2017).
[44] R. Arthur *et al.* (RBC and UKQCD Collaborations), Phys. Rev. D **87**, 094514 (2013).
[45] T. Blum *et al.* (RBC and UKQCD Collaborations), Phys. Rev. D **93**, 074505 (2016).
[46] V. M. Braun *et al.* (QCDSF Collaboration), Phys. Rev. D **79**, 034504 (2009).
[47] S. Sasaki, T. Blum, and S. Ohta, Phys. Rev. D **65**, 074503 (2002).
[48] D. E. Kaplan, M. A. Luty, and K. M. Zurek, Phys. Rev. D **79**, 115016 (2009).